Weak and Strong coupling regimes in plasmonic-QED

T. Hümmer

Instituto de Ciencia de Materiales de Aragon y Departamento de Fisica de la Materia Condensada, CSIC-Universidad de Zaragoza, E-50012 Zaragoza, Spain

F. J. García-Vidal

Departamento de Fisica Teorica de la Materia Condensada, Universidad Autonoma de Madrid, E-28049 Madrid, Spain

L. Martín-Moreno

Instituto de Ciencia de Materiales de Aragon y Departamento de Fisica de la Materia Condensada, CSIC-Universidad de Zaragoza, E-50012 Zaragoza, Spain

E-mail: lmm@unizar.es

D. Zueco

Instituto de Ciencia de Materiales de Aragon y Departamento de Fisica de la Materia Condensada, CSIC-Universidad de Zaragoza, E-50012 Zaragoza, Spain
Fundacion ARAID, Paseo Maria Agustin 36, E-50004 Zaragoza, Spain.

Abstract. We present a quantum theory for the interaction of a two level emitter with surface plasmon polaritons confined in 1D waveguide resonators. Based on the Green's function approach we develop the conditions for the weak and strong coupling regimes by taking into account the sources of dissipation and decoherence: radiative and non-radiative decays, internal loss processes in the emitter, as well as propagation and leakage losses of the plasmons in the resonator. The theory is supported by numerical calculations for several quantum emitters, GaAs and CdSe quantum dots and NV centers together with different types of resonators constructed of hybrid, cylindrical or wedge waveguides. We further study the role of temperature and resonator length. Assuming realistic leakage rates, we find the existence of an optimal length at which strong coupling is possible. Our calculations show that the strong coupling regime in plasmonic resonators is accessible within current technology when working at low temperatures ($\lesssim 4K$). In the weak coupling regime our theory accounts for recent experimental results. Besides, we find highly enhanced spontaneous emission with Purcell factors over 1000 at room temperature for NV-centers. We finally discuss more applications for quantum nonlinear optics and plasmon-plasmon interactions.

1. Introduction

Cavity quantum electrodynamics (cavity QED) was invented to study and control the simplest light-matter interaction: a two level emitter (called TLS or emitter throughout this paper) with a light monomode [1]. At first associated with quantum optics, the emitter was an atom or a collection of them, while the electromagnetic (EM) field was confined in a high-finesse cavity [2]. Nowadays cavity QED experiments cover quite a lot of implementations. Atoms may be replaced by other two level systems, artificial or not, such as quantum dots or superconducting qubits. The light mode can be any single bosonic mode quantized in *e.g.*

superconducting cavities [3], nanomechanical resonators [4], carbon nanotubes [5], photonic cavities [6] or (collective) spin waves in molecular crystals [7].

Cavity QED relies on the comparison between the "light-matter" coupling strength per boson and the irreversible losses from both emitter and bosonic mode. Depending on their ratio two main regimes appear: *weak* and *strong* coupling. In the weak regime losses dominate and the emission spectrum consists of a single peak around the dressed TLS resonant transition while the lifetime is modified because of the field confinement inside the cavity. This modification is nothing but the Purcell effect. In the strong coupling (SC) regime the coupling dominates the losses. In this case a double peak emerges in the emission spectrum, arising from the emitter-resonator level anticrossing. Cavity QED is interesting per se: it demonstrates the quantum nature of both light and matter, and serves *e.g.* for testing quantumness in bigger and complex systems [8]. But, cavity QED is also a resource, e.g. for optimizing single photon emission [9] or lasing [10]. Besides, systems in the SC regime may behave as non linear media [11], generate photon-photon interactions [12] and are the building blocks in quantum information processing architectures [13].

Though weak coupling (WC) regime is relevant, the ultimate goal is to reach the SC regime. The former can be easily reached if the latter is set. Being in the SC regime is determined by the EM field lifetime, confinement and dipole moment. Usually, when working with macroscopic mirrors and atoms having small dipole moments, the field confinement is not optimized but the cavity has extremely long lifetimes, *i.e.* very high finesse or quality factors. In other setups like superconducting circuits all parameters – quality factor, dipole moment and field confinement – are optimized such that the so called ultra-strong coupling regime has been demonstrated [14, 15]. Circuits are promising on-chip setups but have to be operated at microwave frequencies and mK temperatures.

A possible alternative at optical or telecom frequencies, with their plethora of applications in quantum communication, is provided by the subwavelength confined EM fields of surface plasmon polaritons (SPP) in *plasmonic waveguides* [16]. By making resonators out of those waveguides, the energy density and therefore the coupling is highly enhanced. The payoff is that metals introduce considerable losses, further increasing with higher confinement. Therefore, it is not clear under which conditions SC could be reached with plasmonic resonators. On the other hand, advanced architectures of plasmonic waveguides present a good trade off between confinement and losses [17], e.g. hybrid [18], wedge [19] or channel [20] waveguides . Plasmonic waveguides have already shown impressive uses, such as focusing [21,22], lasing [23], superradiance [24], mediators for entanglement between quits [25] and single plasmon emission, [9]. Still, a very challenging perspective is their use for achieving quantum cavity QED with plasmons in the SC regime [26]. Plasmonic QED is not just another layout for repeating what has been done in other cavity QED implementations but offers interesting advantages. As shown in this paper SC can be obtained inside nanometric resonators. It can be mounted *on a chip* in combination with dielectric waveguides. The latter have minor losses but weakly interact with quantum emitters.

In this paper we provide a quantum theory for the coupling between quantum dipoles and resonators made out of one dimensional (1D) plasmonic waveguides. Our theory consistently includes the losses and maps to a Jaynes-Cummings model and, therefore, to the physics and applications of traditional cavity QED. We numerically explore a variety of resonator layouts and several quantum emitters. With all this at hand we set the conditions to reach the SC regime. We also motivate the study of these systems in the less demanding WC regime because of very high achievable Purcell factors into the plasmon channel of more than 1000.

The paper is organized as follows. We first develop the light-matter interaction in plasmon resonators within the Green's function approach. In section 3 the different

realizations for plasmonic resonators and emitters are discussed. We continue in section 4 with numerical results setting the parameter landscape for weak and SC regimes. Section 5 is devoted to emphasize different applications. Some technical details are discussed in the appendices.

2. Interaction of a plasmonic structure and an emitter

2.1. Green's function approach for dissipative field quantization

Surface plasmon polaritons (SPPs or just plasmons) are surface wave quanta bound to the interface between two media characterized by permittivities ($\varepsilon(\omega) = \varepsilon'(\omega) + i\varepsilon''(\omega)$) with real parts of different signs and negative sum. Usually, the interface separates a dielectric ($\varepsilon'(\omega) > 0$) and a metal, which presents $\varepsilon'(\omega) \ll 0$ at optical frequencies, see e.g. Ref [27]. On the other hand, the imaginary part, $\varepsilon''(\omega)$ is responsible for dissipation in the metal (in order to minimize this dissipation, usually the metal used is either silver or gold). Complex permittivities can be easily incorporated in the macroscopic Maxwell equations. However, a problem arises when trying to quantize the EM field: Maxwell equations with a complex permittivity, $\varepsilon''(\omega) \neq 0$, cannot be obtained from a Lagrangian and consequently, a straightforward canonical quantization is not possible. On the other hand, (linear) dissipation can be modeled by coupling the EM field to an additional bath of harmonic oscillators: the system-bath approach [28]. Importantly, the system and bath can be cast to a *total* Lagrangian and consequently this allows the quantization of the EM field in dispersive media [29, 30]. To apply this quantization to complex geometries – needed for plasmonic structures – the theory can be conveniently reformulated by means of the Green's tensor of the classical problem [31–34]. The usefulness of this approach can be appreciated by looking at a key result, the quantum expansion of the electric field

$$\vec{E}(\vec{r},\omega) = i\sqrt{\frac{\hbar}{\pi\varepsilon_0}}\frac{\omega^2}{c^2}\int \mathrm{d}^3 r' \sqrt{\varepsilon''(\vec{r}',\omega)}\overleftrightarrow{G}(\vec{r},\vec{r}',\omega)\left(f^\dagger(\vec{r}',\omega) - f(\vec{r}',\omega)\right) \tag{1}$$

and an analogous expression for the magnetic field. Here, the electric field can be expanded in normal modes where the coefficients are given by the Green's function of the classical field. These normal modes of the combined EM field *and* the dispersive media are represented by theerro bosonic creation (annihilation) operators $f^\dagger(\vec{r},\omega)$ ($f(\vec{r},\omega)$). They obey the commutation relation $\left[f(\vec{r},\omega), f^\dagger(\vec{r}',\omega')\right] = \delta(\omega,\omega')\,\delta(\vec{r}-\vec{r}')$. We used ε_0 to denote the vacuum permittivity and c is the speed of light. Finally, $\overleftrightarrow{G}(\vec{r},\vec{r}',\omega)$ is the dyadic Green's function of the classical field defined by [27, 33]

$$\left[\nabla\times\nabla\times - \frac{\omega^2}{c^2}\varepsilon(\vec{r},\omega)\right]\overleftrightarrow{G}(\vec{r},\vec{r}',\omega) = \overleftrightarrow{I}\;\delta(\vec{r}-\vec{r}')\,. \tag{2}$$

Therefore, within this formalism the quantum fields Eq. (1) are determined by the classical Green's function, Eq. (2).

2.2. Emitter-plasmon interaction

We are interested in the interaction of these quantum fields with a TLS. The actual physical implementation of the emitters will be discussed in detail in section 3.3. In the dipole approximation the interaction can be represented by the emitter's dipole transition strength $\vec{d}$ and the electric field at the position of the emitter ($\vec{r}_e$) [35, Chap. 14]

$$H_{\mathrm{int}} = -\sigma_x \vec{d}\cdot\vec{E}(\vec{r}_e)\,. \tag{3}$$

with $\vec{E}(\vec{r}_e) = \int_0^\infty \mathrm{d}\omega \vec{E}(\vec{r}_e,\omega)$. We use Eq. (1) and define the *collective mode* $\int \mathrm{d}^3 r' \, g(\omega,r',r_e) f(r',\omega) \equiv g(\omega) f(\omega)$. Applying the rotating wave approximation we can write the full Hamiltonian of the emitter coupled to the "field+media" modes as

$$H/\hbar = \frac{\omega_e}{2}\sigma_z + \int_0^\infty \mathrm{d}\omega \; \omega a^\dagger(\omega) a(\omega) + \int_0^\infty \mathrm{d}\omega \left(g(\omega)\sigma^- a^\dagger(\omega) + \mathrm{h.c.} \right) + H_{\gamma_e} \tag{4}$$

This is the *spin-boson* model where the emitter is represented by standard Pauli matrices $\sigma_{x,y,z}$, $\sigma^\pm = \sigma_x \pm i\sigma_y$, and has a level spacing of ω_e. Then, we split these modes in a contribution of modes attributed to plasmonic modes (a), originating from the part of the Green's function that describes propagating plasmons. The coupling to the rest of the modes is encapsulated in H_{γ_e}, eventually responsible for an exponential decay into other channels. The coupling of the emitter to the plasmon modes is characterized by $|g(\omega)|^2$, also called *spectral density* and can be expressed by noticing that, $\left[f(\omega), f^\dagger(\omega') \right] = \delta(\omega,\omega') \rightarrow |g(\omega)|^2 = \int d^3 r' \, |g(\omega,r',r_e)|^2$ together with a property of the Green's function by [27, 31]

$$|g(\omega)|^2 = \frac{1}{\hbar \pi \varepsilon_0} \frac{\omega^2}{c^2} \vec{d}^T \, \mathrm{Im}[\overleftrightarrow{G}_{\mathrm{spp}}(\omega,\vec{r}_e,\vec{r}_e)] \vec{d}. \tag{5}$$

Here, $\overleftrightarrow{G}_{\mathrm{spp}}$ is the part of the Green's tensor attributed to plasmons in the nano-structure. Finally, we mention that we work in the regime that coupling to the non-radiative channels (H_{γ_e}) is weak and non-resonant. Thus, it will be modeled by phenomenologically decay rates,

$$\gamma_e = \gamma_{\mathrm{rad}} + \gamma_{\mathrm{int}} + \gamma_{\mathrm{nonrad}} \, . \tag{6}$$

Emission into free space radiating EM modes is depicted by γ_{rad}. Internal loss processes in the emitter, such as non-radiative electron-hole recombinations in quantum dots, are quantified by γ_{int}. Furthermore, another emitter loss channel specific to plasmonic structures arises. If the emitter is placed close to a metal surface, it couples to non-propagating, quickly decaying evanescent modes and the energy is dissipated through heating of the metal. The associated rate will be called γ_{nonrad} and can assume very high rates when an emitter is close to a metal surface [36, 37] . To avoid the latter, one may lift the TLS away from the metal surface, and place it at an intermediate region close enough to still couple efficiently to plasmons.

2.3. Green's function of plasmonic structure

A strategy for confining the EM field to a small area, and consequently enhance light-matter interaction, is by using one dimensional metallic structures (waveguides) that support propagating plasmons. The plasmonic modes of the waveguide confine the EM field in two dimensions. Since they are mixed photon-media excitations, the confinement can exceed the one of free space photons that is limited by diffraction. To further enhance the interaction the plasmons can be stored in *resonators*. These can be manufactured out of plasmonic waveguides by placing two mirrors or building a ring, see Fig. 1 for a sketch.

2.3.1. Waveguide Surface plasmons on an infinite *open* waveguide can be described by $\vec{E}(\vec{r}) = \vec{E}(\vec{r}_t) e^{\pm i k(\omega) z}$, with the transverse field profile $\vec{E}(\vec{r}_t)$ where z is the coordinate parallel and $\vec{r}_t \equiv \{x,y\}$ perpendicular to the waveguide. Due to propagation losses of the plasmons, their propagation constant $k(\omega) = k'(\omega) + i k''(\omega)$ is a complex quantity. The Green's function $G_{\mathrm{spp}}(\omega,\vec{r},\vec{r}')$ can be constructed out of the (approximately) orthogonal electric field modes [38, 39]

$$\overleftrightarrow{G}_{\mathrm{spp}}(\omega,\vec{r},\vec{r}') \approx \frac{c^2}{\omega v_g} \frac{\vec{E}(\vec{r}_t) \otimes \vec{E}^*(\vec{r}_t')}{\int_{A_\infty} d^2 \tilde{r}_t \varepsilon(\tilde{\vec{r}}_t) \left| E(\tilde{\vec{r}}_t) \right|^2} k G_{1\mathrm{d}}(\omega,z,z') \tag{7}$$

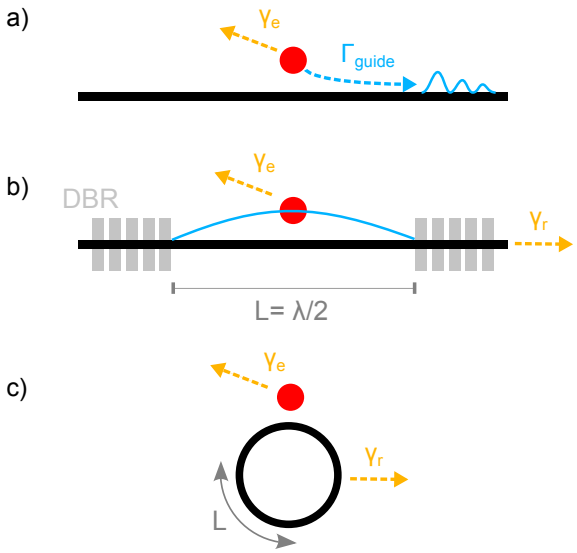

Figure 1. (a) Sketch of an emitter (red dot) coupled to an open plasmonic wave guide. It emits with rate Γ_{guide} into propagating surface plasmons and with rate γ_e into other modes. (b) Linear resonator defined by a waveguide enclosed by mirrors (here distributed Bragg reflectors, DBR). The excitations from the resonator are lost with rate γ_r. The length of the resonator has to be multiples of half the plasmon wavelength for resonances to occur. (c) A circular resonator configuration.

where the speed of light and group velocities are c and $v_g(\omega) = \partial\omega/\partial k$ ‡ respectively. This is the Green's function of the bound surface plasmons for the area outside of the metal. The formula is split in a part perpendicular to the waveguide and a part along the waveguide, $G_{1\text{d}}$, that matches the 1D (scalar) Green's function [40, Chap. 2]

$$G_{1\text{d}}(\omega, z, z') = \frac{i}{2k} e^{ik|z-z'|}. \tag{8}$$

Evaluating the coupling strength $g(\omega)$ at the optimal position in the waveguide, using Eq. (5) and Eq. (8) we get

$$|g(\omega)|^2 = \frac{1}{2\pi}\Gamma_0 \frac{3}{\pi\varepsilon_d^{3/2}} \frac{c}{v_g} \frac{A_0}{A_{\text{eff}}} \equiv \frac{1}{2\pi}\Gamma_{\text{guide}}\,, \tag{9}$$

where Γ_0 is the "free space spontaneous emission", $\Gamma_0 = \varepsilon_d^2\omega^3|d|^2/3\pi\hbar\varepsilon_0 c^3$ if the emitter is placed in a homogeneous medium with permittivity ε_d and we finally we define Γ_{guide} to be the emission rate into surface plasmons of the open waveguide. Here, ε_d is the permittivity of the dielectric the emitter is placed in. The diffraction limited area in vacuum, $A_0 = (\lambda_0/2)^2$, is the minimum area light of wavelength λ_0 can be confined to in vacuum. Furthermore, we introduced the effective mode area of the plasmon field

$$A_{\text{eff}}(r_t) = \frac{\int_{A_\infty} d^2\tilde{r}_t \varepsilon(\tilde{\vec{r}}_t)\left|E(\tilde{\vec{r}}_t)\right|^2}{\max\{\varepsilon(\vec{r}_t)\left|E(\vec{r}_t)\right|^2\}}. \tag{10}$$

It is inversely proportional to the maximum energy density and therefore quantifies the achievable coupling strength.

‡ Through this work we compute v_g numerically by evaluating the derivative: $v_g(\omega) = \partial\omega/\partial k$.

2.3.2. Resonator In a resonator, the 1D Green's function can be obtained by summing all the reflected contributions of a wave originating from a $\delta-$source [40, 41]. The details can be found in Appendix B. We will look at two resonator configurations. Either a linear resonator of length L terminated by two mirrors with reflectivity $|R|$ or a circular resonator with circumference L.

In both configurations the spectral density $|g(\omega)|^2$ is peaked around the resonance frequencies $\omega_r = 2\pi v_p/\lambda$ as shown in Fig. 2. Here, v_p is the phase velocity and $\lambda = \lambda_0 v_p/c$ the wavelength of the SPPs. The condition for resonance is

$$L = \frac{\lambda}{2}m = \frac{\pi v_p}{\omega_r}m \tag{11}$$

Where m counts the number of the field antinodes in the resonator and has to be an even integer for circular resonators and any integer for the linear configuration.

In a real system, the resonator will have losses, with different contributions that can be encapsulated in the coefficient γ_r

$$\gamma_r = 2v_g\left(k''(\omega_r) - \frac{1}{L}\ln|R|\right) \equiv \gamma_{\text{prop}} + \gamma_{\text{leak}}\,. \tag{12}$$

where γ_{prop} are plasmon propagation losses and γ_{leak} leakage through the mirrors in the linear resonator. For the circular resonator radiative losses due to bending have to be added but will not be treated in detail here.

Taking into account losses, the spectral density can be approximated close to the resonant frequency by (see Fig. 2, and Appendix B for a derivation)

$$|g(\omega)|^2 \approx g^2\frac{2}{\pi}\frac{\gamma_r\omega_r\omega}{(\omega^2-\omega_r^2)^2+\gamma_r^2\omega^2} \tag{13}$$

where we assumed that the resonator linewidth is small compared to the resonance position, $\gamma_r \ll \omega_r$, i.e. we have a well defined resonance. The coupling amplitude is given by

$$g = \sqrt{\Gamma_{\text{guide}}\frac{v_g}{L}}\,. \tag{14}$$

We assumed that the emitter is positioned at a field antinode in the linear resonator to yield maximum coupling. In the circular resonator the emitter can be placed anywhere along the waveguide.

Let us comment on the dependence $\gamma_{\text{leak}} \sim 1/L$. Notice that γ_{leak} is the energy loss *per time* through the resonators mirrors. Therefore the leakage must be proportional to the energy density at the mirrors which is $\sim 1/L$. In a proper resonator with highly reflective mirrors we can expand $-\ln|R| \equiv -\ln(1-|T|) \cong |T|$ for small transmission and absorption coefficients, $|T| \ll 1$. Thus, the leakage is proportional to the transmittance. In contrast to the leakage, the propagation losses γ_{prop} do not depend on the resonator length since the linewidth (and the loss rate) quantify the losses *per unit of time* and not per resonator round-trip of the plasmons. The propagation losses are proportional to the imaginary part of the plasmon wavevector k'' or, in other words, inverse to the plasmon propagation length defined as $\ell \equiv 1/(2k'')$.

2.4. The JC-model: Plasmonic QED

We now use a mathematical result with an enormous physical relevance: The bosonic bath coupled to a TLS with a peaked spectral density, $|g(\omega)|^2$ like Eq. (13) can be split in a single boson mode with frequency ω_r, coupled to a bath characterized by a dissipation rate γ_r, *i.e.* the $|g(\omega)|^2$ width [42–45]. Physically, the ω_r-mode is the single resonator mode. In the end,

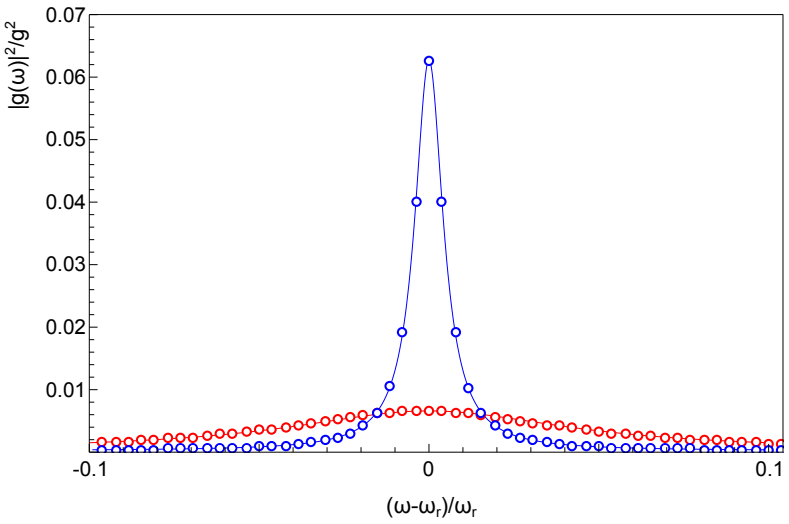

Figure 2. Spectral density $|g(\omega)|^2$ of the resonator for different losses (blue $\gamma_r = 0.01\omega_r$ and red $\gamma_r = 0.1\omega_r$). The solid line is the exact spectral density of a resonator following Eq. (B.4) while the circles are the approximation with Eq. (13).

the plasmonic resonators discussed here can now be approximated by the Jaynes-Cummings model

$$H_{\rm JC}/\hbar = \frac{\omega_e}{2}\sigma_z + \omega_r a^\dagger a + g\left(\sigma_- a^\dagger + \sigma_+ a\right) \tag{15}$$

with additional losses from the emitter (with rate γ_e) and from the resonator (with rate γ_r). This physics can be encoded in an *Optical Master Equation* for the density matrix ρ, after tracing out the bath degrees of freedom. It takes the form of the celebrated *Markovian Lindblad* master equation [46, 47],

$$\begin{aligned}\dot{\rho} = &-\frac{i}{\hbar}[H_{\rm JC},\rho] \\ &+\gamma_r\left(a\rho a^\dagger - \frac{1}{2}\left\{a^\dagger a,\rho\right\}\right) + \gamma_e\left(\sigma_-\rho\sigma_+ - \frac{1}{2}\left\{\sigma_+\sigma_-,\rho\right\}\right) + \frac{\gamma_d}{4}\left(\sigma_z\rho\sigma_z - \rho\right).\end{aligned} \tag{16}$$

Here, we have also introduced an additional phenomenological pure dephasing term γ_d that models broadening of the spectral emission observed in solid state emitters, by *e.g.* coupling to phonons [48–52].

This is the expected and desired result. Making resonators out of waveguides pursues building cavity-QED systems. As a consequence many of the results from Jaynes-Cummings physics in cavity QED can be imported to quantum plasmonic systems. We emphasize that, within the formalism sketched here, the master equation has been obtained from a *first principles* theory. Therefore, parameters like the coupling between the single plasmon resonator mode and the emitter, g, and the decoherence rates γ_r and γ_e can be computed from the emission spectra of the qubit and the Green's function of the plasmonic structure.

3. Realization of plasmonic QED

In this section we specify the actual emitters and resonator architectures studied in this work.

3.1. Waveguides

The plasmon resonators treated in this work are made out of waveguides. Therefore, the final resonator properties depend critically on the specific waveguides used, especially on the achievable field confinement and plasmon propagation length. Plasmon waveguides are quasi-1D translational invariant metal-insulator structures. They possess propagating SPP-eigenmodes with exponentially decaying evanescent fields in both the metal and the dielectric. The waveguides we focus at may reach high field confinements along with low propagation losses. Usually there is a trade-off between confinement and propagation length, but the actual values are geometrically dependent. We pick three different waveguide geometries which offer long propagation lengths along with high field confinements, as well as good fabrication techniques: The first type are small diameter metal *nanowires* [16]. The second type are sharp metal *wedges* [19,53] offering high field strengths at their tips. Finally, the third class are *hybrid* waveguides [18, 23], formed by a high refractive index dielectric nanowire (silicon $\varepsilon = 12.25$) placed close to a metal surface. There, the SPP of the plane and the mode of dielectric create a hybrid mode with strong field confinement in the gap. Transversal cuts through the three waveguides are plotted in Fig. 3 along with a sketch of their field energy distribution. The propagation length and confinement of these waveguides depend on the concrete geometrical parameters of the waveguides. In the hybrid waveguide the main parameter is the gap size between the dielectric and the metal surface. The nanowire properties depend on the radius and the wedge on the tip angle and the tip radius. For smaller wires, smaller gaps or tighter angles, respectively, the field confinement increases and the propagation lengths decrease. Finally, we consider that the metal waveguides are made of silver, which offers best propagation lengths at optical and telecom frequencies and are embedded in PMMA ($\varepsilon_d = 2$).

3.2. Resonators

In our calculations we consider two architectures, a *circular* and a *linear* resonator as sketched in Fig. 1.

3.2.1. Circular resonator The circular resonator is formed by bending a waveguide and connecting its ends. The fundamental disadvantage is that the energy is converted from propagating modes to free radiation at bending [54, 55]. On the other hand these losses decrease exponentially with increasing the radius of the ring. Moreover it is expected that bending losses are smaller for higher confined modes. Circular waveguides cannot be yet build using chemically synthesized nanowires and one has to reside to lithographically built waveguides, which offer worse propagation lengths due to their polycrystalline nature and the associated radiative and non-radiative losses at domain interfaces.

3.2.2. Linear resonator Linear resonators can be built by placing reflective mirrors in the waveguide. Here scattering losses and transmission through these mirrors have to be avoided for having good resonators. Although distributed Bragg reflectors were predicted to be limited to low reflectivities for plasmons on 2D metal surfaces [56], recent resonator realizations showed high reflectivities when using modes highly confined to waveguides and alternating dielectric layers with small refractive index differences [9]. In comparison to optical and microwave cavities, where mirror absorption, scattering and transmission losses can be reduced to several ppm [57, 58], plasmon mirrors are expected to exhibit losses in the order of a few percent.

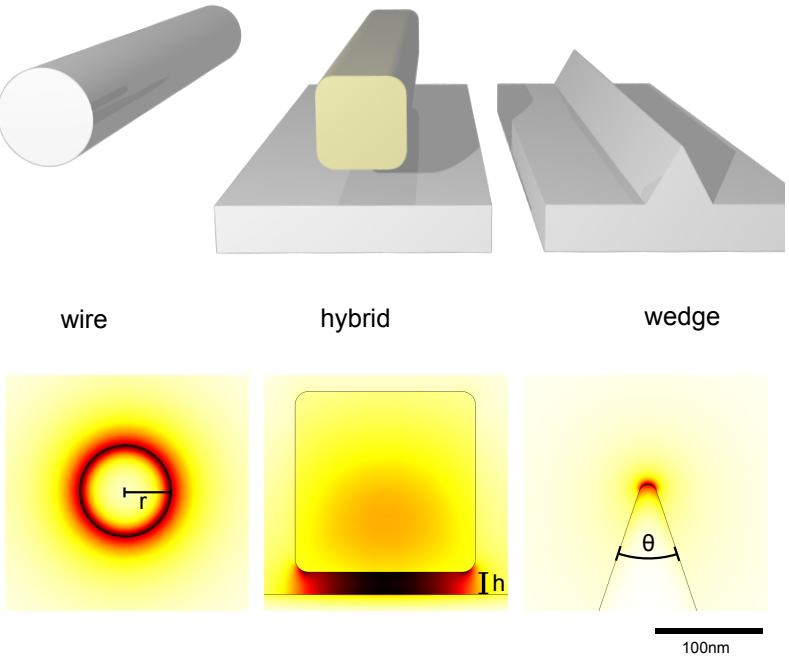

Figure 3. Model of the three waveguides treated in this work. Below the relative energy density of each waveguide is sketched. The parameters used here are $r = 50$nm, $h = 25$nm, $\theta = 40°$ and the SPP eigenmodes are numerically computed for a frequency corresponding to a free space wavelength $\lambda_0 = 1550$nm.

3.3. Quantum emitters

Emitters should be photostable with a high dipole moment to interact strongly with the resonator field and ideally should be embeddable into a solid state substrate or on top of a surface without destroying them. Interesting candidates are color centers in crystals or semiconductor quantum dots (QDs) grown on surfaces or chemically synthesized as nano-spheres.

The emission spectrum of single atomic emitters traditionally studied in quantum optics is simply a Lorentzian with a very narrow *transform limited linewidth* given by the time-energy uncertainty relation. In contrast, solid state emitters have higher dipole moments but are also coupled strongly to their solid state environment. Therefore, the transform limited line, also called zero-phonon-line (ZPL), is dominated and covered by phonon sidebands, giving rise to a very broad non-transform limited spectrum [48, 50, 52, 59]. As used in section 2.2, this broad peak can be modeled phenomenological by an additional source of dephasing in the master equation (16) [48–52]. At lower temperature the phonon sidebands mostly vanish and the ZPL can be observed.

The first emitter we consider is nitrogen-vacancy(NV) centers in diamond [60]. At room temperature(RT) a single center can be found embedded in diamond nanocrystals of sizes down to a few nm. They feature high stability and at room temperature a about 80 nm broad (FWHM) peak centered around ≈ 670 nm. The strong overall dipole moment (including RT sidebands) is responsible for a spontaneous emission rate of 0.04 GHz at room temperature. At lower temperatures (2 K) the ZPL prevails at 638 nm with an spontaneous emission of 0.013 GHz. NV-centers are interesting due to their stability, homogeneous properties and

long spin coherence times, making them ideal for quantum information processing tasks as has been recently reviewed in Ref. [60].

The second emitter we investigate are chemically synthesized CdSe semiconductor quantum dots. These spherical nanocrystals with diameters around several nm can also be operated at RT and show a size-tunable emission wavelength in around the red spectrum. An example is a quantum dot with a $\approx 20\,$nm broad peak at $650\,$nm [61, 62] and spontaneous emission of $0.05\,$GHz at room temperature [62] . Finally, we study quantum dots made out of InAs clusters in GaAs [63,64]. They can exhibit very strong dipole moments and spontaneous emission rates above $1\,$GHz at cryogenic temperatures ($T \sim 4K$).

4. Weak and strong coupling

4.1. Strong coupling condition

The eigenvalues of (15) form the so called JC-ladder. At resonance $\omega_r = \omega_e$, the states split in doublets $|\psi_\pm\rangle = 1/\sqrt{2}(|N,g\rangle \pm |N-1,e\rangle)$ with energies $E_{n,\pm} = \hbar N\omega_0 \pm \hbar\sqrt{N}g$. The degeneracy between TLS and resonator is lifted because of the coupling yielding an anticrossing split by $2g\sqrt{N}$. Considering the smallest level repulsion with one photon, $N = 1$, the SC condition is usually settled as the parameter range where such anticrossing can be resolved in an emission spectrum. Furthermore, the spectral lines are broadened because of the losses and therefore the strong coupling regimes imposes that g overcomes dissipation and decoherence. This is the case if [65, 66]

$$|g| > \frac{1}{4}|\gamma_r - \gamma_e|\,. \tag{17}$$

Here we neglected emitter dephasing. In the opposite case, the losses dominate over the coupling and the lines can not be resolved. This is the the WC regime.

Reaching the SC is *the* objective in many cavity QED experiments. From the fundamental point of view resolving the $|\psi_\pm\rangle$ states confirms the quantum nature of the light-matter coupling. Being in the SC regime has multiple practical applications as well, that we will discuss to some extent in the next section for the case of plasmons. Nevertheless, the WC regime has its own interest, *e.g.* for effective single photon generation. In both cases the ratio of coupling over losses should be as large as possible. In the following we compute the coupling and losses in the case of different plasmonic resonators. The number of parameters to play is huge so a *brute force* exploration seems a waste of time. Therefore we first look at the dependencies of both the coupling and losses and work in optimal configurations.

From Eq. (14) we see that $g \sim \sqrt{\Gamma_0/(A_{\rm eff}L)}$. The coupling strength depends on the emitter, via its free space spontaneous emission and therefore its dipole moment $\Gamma_0 \sim |d|^2$. Larger dipole moments directly translate to higher couplings. The two remaining dependencies come from the resonator itself. The first one is the transverse field confinement $\sim 1/A_{\rm eff}$. The very small mode area of plasmons was the motivation to investigate plasmon resonators in the first place. Finally, the coupling depends on the field strength at the emitter position and consequently $g \sim 1/\sqrt{L}$.

Now we turn to the right side of the SC condition, Eq. (17), quantifying decoherence of emitter and resonator. To minimize resonator losses in Eq. (12) we must search for long propagation lengths and highly reflective mirrors. Besides, we see an interesting dependence with $1/L$ in γ_{leak} [Cf. Eq. (12) and discussion below]. This must be compared to the $1/\sqrt{L}$ dependence of the coupling strength. Therefore, in a realistic scenario where the reflectivity is always less than one, these two dependencies compete and depending on the other parameters an optimal length appears. This discussion is also true for the ring configuration by replacing

leakage through the mirrors by bending losses. The latter also decreases when increasing the resonator length (but this time exponentially [55]) since the curvature is reduced. Therefore, pretty much like in the linear case, for circular resonators an optimal length also appears.

4.2. Temperature and propagation losses

In the next section we will see that the losses from the plasmon resonators are often dominated by the small propagation length of the plasmons. In particular, it may not be sufficient to use sophisticated waveguide geometries to increase this length. An often overlooked factor affecting plasmon propagation length is temperature, since usual plasmonic experiments are operated at room temperature. However, lowering the temperature, the propagation length of plasmons can be systematically extended by orders of magnitude [26]. This increase is possible if the conduction losses inside the metal are dominated by scattering at phonons instead of defects like grain boundaries or impurities. Furthermore, the metal nanostructure must have a smooth surface or otherwise electron scattering at the surface will dominate [16, 67](as well as radiative losses but they are much smaller [16]).

Using the Drude-Sommerfeld model for free electrons, the imaginary part of the permittivity, ε'' is approximately proportional to the resistivity, ρ (details in Appendix D). Since the $|\varepsilon'| \gg |\varepsilon''|$ the modal properties of the plasmons are not affected and an decrease in resistivity directly translates into an increase in propagation length

$$\ell \propto \frac{1}{\varepsilon''} \propto \frac{1}{\rho\,(T)}\,. \tag{18}$$

Working at lower temperatures is of course an experimental hurdle. However, since many quantum emitters are operated at lowered temperatures anyway, it may already be needed for an envisioned setup. In sufficiently smooth, pure and single crystalline silver, the propagation length can be easily enhanced by a factor of about 10 when using liquid nitrogen (77 K) or even almost 100 when using liquid helium (4 K), see Appendix D.

4.3. Strong and weak coupling in plasmon resonators

Now we want to get an systematical overview if the SC condition (17) can be fullfilled with combinations of realistic plasmon waveguides, resonator geometries and emitters. Since this depends on so many adjustable parameters (different waveguides each with different geometries, resonator reflectivity and length, temperature, emitters) we try to get insight in a plot that gives an broad overview for as much as possible of these parameters. To this end we rearrange the SC condition [Eq. (17)] as

$$\sqrt{\frac{3}{m}\frac{\Gamma_0}{\omega}\frac{v_p c}{v_g^2}\frac{A_0}{A_{\text{eff}}}} > \frac{1}{8}\left(\frac{\ell}{\lambda}\right)^{-1} - \frac{1}{2m}\ln|R|\,. \tag{19}$$

We neglected the emitter losses and furthermore we used the relation $\omega = v_p k$. Notice that , the properties of the waveguide are encoded in only two parameters: one proportional to the field confinement $\frac{v_p c}{v_g^2}\frac{A_0}{A_m}$ and the other one being the propagation length normalized to the plasmon wavelength ℓ/λ. Hence, we choose this to be the axis of a 2D-plot [17] in Fig. 4 and then can overlay borders separating strong and weak coupling independent of the actual waveguide used. The waveguides differ in their fundamental type (nanowire, hybrid, wedge) and we vary the geometrical parameters to see a broad range of achievable field confinements and propagation lengths. Furthermore, we mark the border between strong and weak coupling for various resonator lengths ($L = m\lambda/2$, see Eq. 11) and mirror reflectivities ($|R|$) overlaid

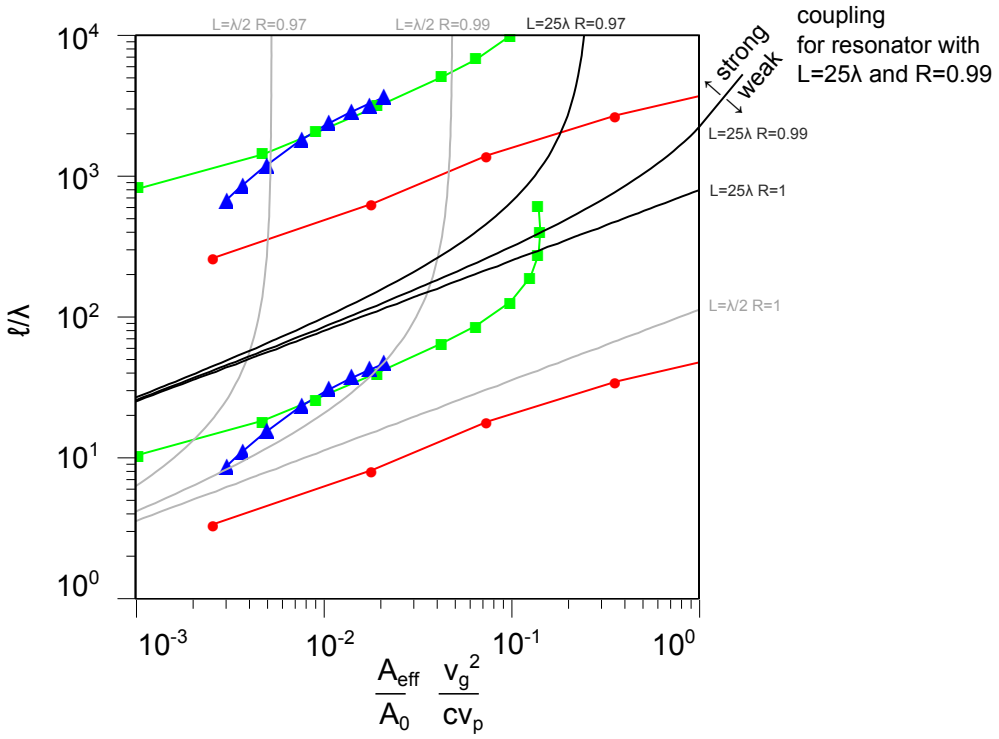

Figure 4. Overview of different wedge(▲) , hybrid(■) and nanowire(●) waveguides for reaching SC. The emitter has $\lambda_0 = 1550\,\text{nm}$ and $\Gamma_0 = 1\,\text{GHz}$. We draw lines separating the region of strong and weak coupling for multiple resonator realizations with different lengths ($L = \{\lambda/2, 25\lambda\}$) and end reflectivities ($R = \{1, 0.99, 0.97\}$). The parameters of each waveguide are varied to yield different confinements and propagation lengths. We chose the following parameters for the waveguides, marked by symbols, starting from the bottom left point of the individual waveguide lines: The nanowire waveguide has radii of $r_{rad} = \{25, 50, 100, 250, 500, 750, 1000\}\,\text{nm}$. The wedge waveguide angles of $\theta = \{5, 10, 20, 40, 60, 80, 100, 120\}^\circ$ and its tip has a radius of 10 nm. The hybrid waveguide has separations between the metal and the dielectric nanowire of $h = \{5, 25, 50, 100, 200, 300, 500, 750, 1000, 1250, 1500\}\,\text{nm}$ and a the dielectric nanowire width of 200 nm. Furthermore we plotted the waveguides operated at room temperature (lower three lines) and 4K (upper three lines).

on our plot for the waveguides. If a certain waveguide point lies at the top (meaning higher propagation length than the minimum required) and left (meaning higher confinement than needed) of a respective line then the emitter and the resonator made of this waveguide are in the SC regime.

The calculations of propagation length and field confinement was carried out numerically via a finite element method and the the emitter was considered to be located at the optimal point of maximum field strength.

In Fig. 4 a strong emitter operating at telecom frequencies (free space wavelength $\lambda_0 = 1550\,\text{nm}$) was assumed, e.g. a self assembled InAs/GaAs quantum dot. As we can see, SC is hard to achieve. With non perfectly reflecting mirrors ($R = 0.99$) only the hybrid waveguide with the is in the area of SC. The wire and the wedge waveguide are always in the WC . Lines operated at lowered temperatures, 4K are shifted upwards to two orders of magnitude longer propagation lengths. Of course, imperfections in the waveguides may limit

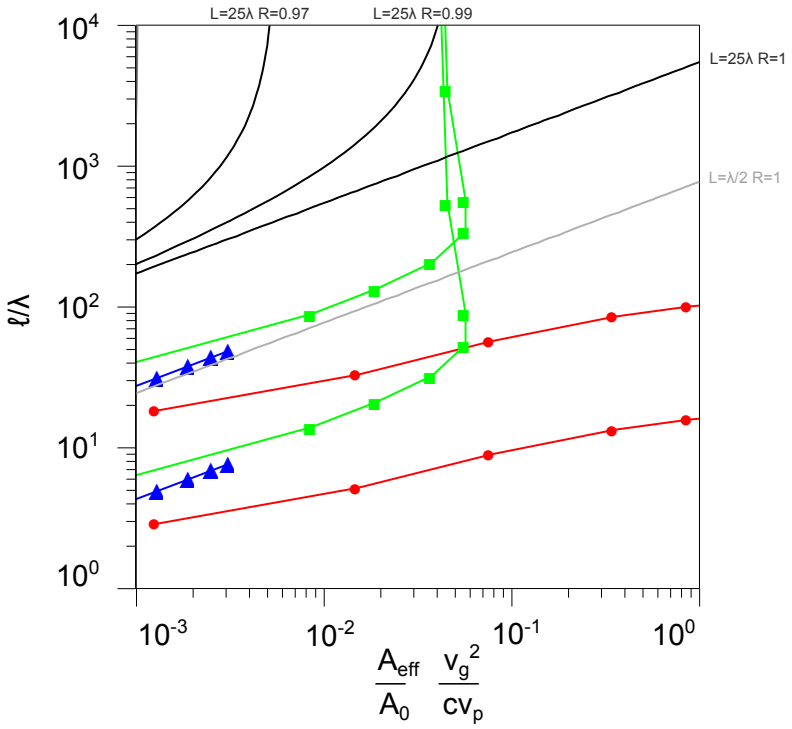

Figure 5. Same plot as in Fig. 4 but with an emitter operating at $\lambda_0 = 650\,\text{nm}$ and a free space spontaneous emission rate of $\Gamma_0 = 0.05\,\text{GHz}$. This roughly corresponds to CdSe QDs or NV-Centers. The waveguide properties are all the same as in Fig. 4 except the dielectric nanowire that has been adapted to better perform at this wavelength with a width of 100 nm.

such enhancements in propagation length. However, we see that even at lower propagation length increases we are comfortably in the SC regime, either with good reflective ends or longer resonators.

We can conclude here that for high-dipole moment quantum dots (e.g. InAs/GaAs) that are operated at lowered temperatures anyway, strong coupling should be reachable. This is possible by using (chemically synthesized) smooth single-crystalline waveguides, realistic DBR mirror reflectivities above 95% and resonator lengths of several wavelengths. The straight borders in Fig. 4 with $\{L = 25\lambda, |R| = 1\}$ may correspond to a circular resonator long enough to neglect bending losses.

4.4. NV-Center or CdSe QDs

In Fig. 5 we plot the same as in Fig. 4 but for emitters with spontaneous emission of $\Gamma_0 = 0.05\text{GHz}$ at $\lambda_0 = 650\text{nm}$. This resembles optimistic values for CdSe QDs or NV-centers. In this case the SC regime is harder to reach: the emission rate is smaller and the normalized propagation length of most of the waveguides is shorter at optical than at telecom frequencies . Even at lowered temperatures reaching SC with emitters with such low emission rates presents an experimental challenge. Especially since at optical frequency interband transitions, which are independent of temperature, limit the achievable propagation length increase.

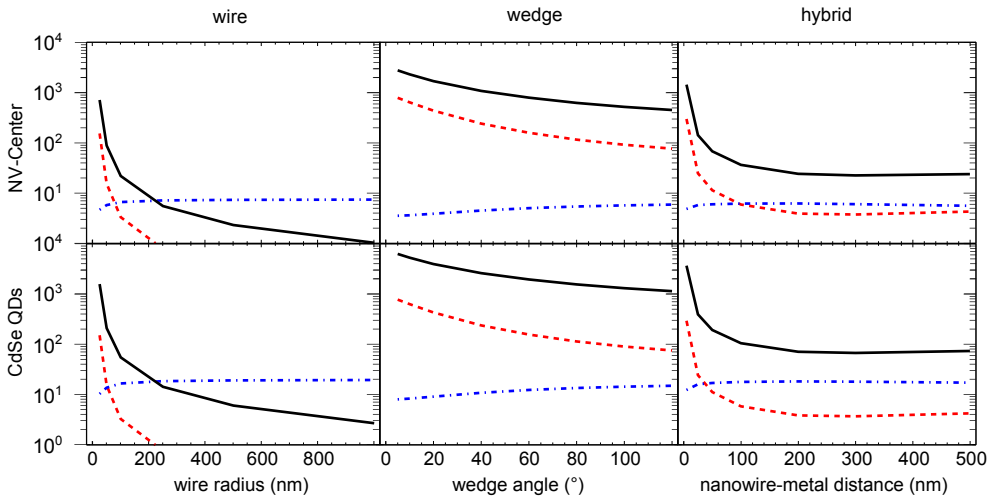

Figure 6. Purcell factors for plasmon resonators made of different waveguides. The emitters used are NV-Centers and CdSe QDs *at room temperature* with a a free space wavelength of approximately 650nm. The reflectivity of the resonator ends is $|R| = 0.97$ and its length $L = \lambda/2$. The red dashed line is the Purcell factor due to transverse mode confinement of the guided modes (F_{guide}). The blue dashed-dotted line is the Purcell factor originating from the resonator (F_{res}). The solid black line is the total Purcell factor. For higher confined modes (left side of each plot), the resonator Purcell factor decreases since the higher losses decrease the resonators Quality factor. For weakly confined long propagating modes (right side of the plots) the resonator Purcell factor is limited by the emitter's quality factor.

4.5. Tradeoff between Confinement and losses

In Fig. 4 we first notice the well-known tradeoff between mode confinement and propagation length for plasmon waveguides [68]: The parametric lines for each waveguide run more or less diagonal from bottom left to the right top of the 2D plot. However, the individual waveguide types perform different with the hybrid waveguide offering highest field confinement and propagation lengths as noted in Ref. [17]. The mode confinement in the plane perpendicular to the waveguide therefore affects the maximum achievable quality factor of the resonator.

Interesting enough, we see the same trend as for plasmon waveguides also exists for the whole resonators as well: the stronger the field confinement in the dimension *along* the waveguide – e.g. shorter resonators – the higher are the losses through the ends of the resonators. This is also true for circular resonators, where building shorter but stronger bent resonators results in higher bending losses.

5. Applications

Let us discuss some practical applications of the theory presented so far.

5.1. Purcell enhancement for single plasmon sources

As derived in Appendix C the Purcell factor for plasmon resonators, *i.e.* emission into surface plasmons compared to the emission if the emitter would be placed in a homogeneous dielectric

with ε_d, is

$$F = F_{\text{guide}} \times F_{\text{res}} = \frac{3}{\pi \varepsilon_d^{3/2}} \frac{c}{v_g} \frac{A_0}{A_{\text{eff}}} \times \frac{4}{m\pi} \frac{v_g}{v_p} \frac{1}{\frac{1}{Q_d} + \frac{1}{Q_r}} . \tag{20}$$

The first part is a broadband enhancement due to strong transversal field confinement ($\propto A_{eff}^{-1}$) and slow light ($\propto v_g$) in plasmonic waveguides. The second part is a resonant wavelength dependent enhancement arising from the longitudinal confinement in the resonator.

At room temperature, the solid state emitters presented in section 3.3 exhibit broad bandwidths due to dephasing. This can be efficiently expressed in terms of the Quality factor of the emitter, $Q = \lambda_0/\Delta\lambda$, where $\Delta\lambda$ is the linewidth of the emitter almost entirely attributed to dephasing. For popular emitters like NV-centers and CdSe quantum dots the Quality factors are $Q_{d,\text{NV}} \approx 670\text{nm}/80\text{nm} \approx 8$ and $Q_{d,\text{CdSe}} \approx 650\text{nm}/20\text{nm} \approx 33$, respectively [60,61]. These values are considerably smaller than those for typical plasmon resonators and therefore limit the achievable Purcell factors. This can be understood if we visualize that the linewidth of the resonator is much smaller than the one of the emitter, therefore being only resonant with a small part of the emitter emission spectrum. The advantages of plasmon resonator are that the sub-wavelength field confinement allows a very high broadband enhancement [9, 69, 70]. Indeed, as we can see in Fig. 6 the Purcell factor due to transversal mode confinement is responsible for very high overall Purcell factors. This is even true for very broad emitters at room temperature where Purcell factors above 1000 are possible. We especially see that the decrease in propagation length of higher confined modes plays no role here: the enhancement of the broadband Purcell factor due to mode confinement exceeds the decrease of the resonant Purcell factor due to the reduction in propagation length.

In a recent experiment [9] Purcell factors of 75 have been reported for CdSe QDs when coupled to a 50 nm radius nanowire embedded in PMMA. Taking the experimental reported parameters for $L = \lambda$ terminated by DBR mirrors with reflectivities ≈ 0.95 we get a Purcell factors between 107 and 64 when varying the QD distance to the wire surface between 0 nm and 10 nm. This is a very good agreement with the reported value, especially when taking into account that we have not fitted any parameter.

Furthermore a look at lowered temperatures is also interesting here. Magnitude higher Purcell factors can be expected through higher Quality factors of cavities and emitters at lower temperatures.

Although the cavity Purcell factor is lower than the broadband Purcell factor for highly confined waveguides, it has several features that are important for single plasmon sources. First of all, it still has a value above 5 for the broadband emitters in Fig. 6 and therefore is a significant contribution to the high overall Purcell factor. Second, it selectively enhances plasmons with large propagation lengths, since it is an effect attributed to cavity resonance. Only the SPPs which match the cavity length are enhanced. This is particular important when dealing with the "efficiency" to emit radiation into this SPPs.

5.2. Strong coupling

Once we know under which conditions the SC regime is reachable within plasmonic resonators, we go through some applications. As anticipated in the introduction, cavity QED systems in the strong coupling are a cornerstone in quantum optics and a huge number of applications were proposed and implemented in different realizations. Let us discuss some of them that may have relevance in the manipulation of light at the nanoscale. All those applications are implicitly or explicitly related to the coherent coupling between the TLS and the resonator mode, encapsulated in the ratio, g/ω_r and $g/\max[\gamma_r, \gamma_e, \gamma_d]$. The larger the

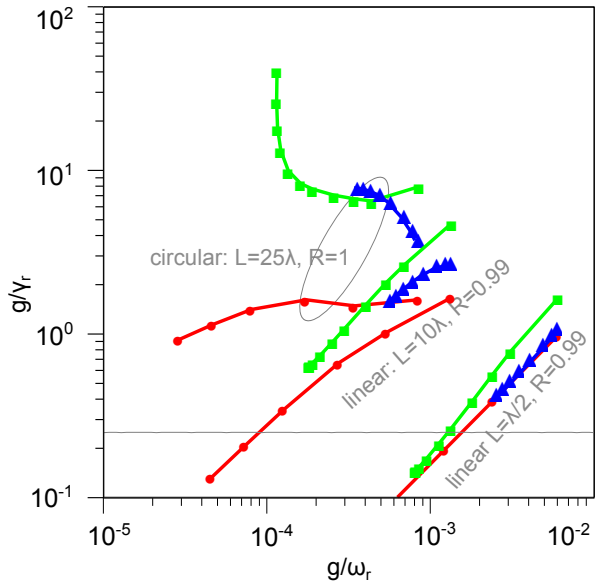

Figure 7. Coupling strength over losses for an $\Gamma_0 = 1\,\text{GHz}$ emitter at $\lambda_0 = 1550\,\text{nm}$ at $4\,\text{K}$ for different waveguide-resonator combinations.

coupling and smaller the losses, the faster and more coherent light-matter oscillations are, optimizing the performance of many of the applications. For later reference, we plot the expected performance of g/γ_r for several plasmon resonators in Fig. 7, operated at 4K. The waveguides plotted include a long and a short linear resonator with reflectivity of $|R| = 0.99$ and a sufficiently long circular resonator where we assumed that bending losses can be neglected. The emitter properties are taken from section 4.3 (e.g. InAs/GaAs QDs).

Quantum nonlinear optics The JC-model (15) is nonlinear , the energy levels are not equally spaced. Therefore, its response to an external stimulus, is not linear as well. In the dispersive regime [71], by expanding the JC-model in powers of $g/\delta \ll 1$ with $\delta = \omega_r - \omega_e$, effective Kerr Hamiltonians like $H/\hbar = \omega a^\dagger a + \kappa(a^\dagger a)^2$, have been proposed [72]. Kerr nonlinearities generate squeezed states. In a circuit-QED implementation such physics have been recently reported [11]. In that work the authors exploited these nonlinearities to demonstrate, among other things, squeezing. In this experiment $g/\gamma_e \sim 10$ and $g/\omega \sim 10^{-3}$. As shown in Fig. 7, these numbers can be reproduced with the plasmonic resonators considered in this paper.

Plasmon-plasmon interaction Rooted in the same nonlinearities, the JC-physics can be used to induce effective photon-photon interactions, as in the so-called photon blockade phenomenon [73]. Another evidence for photon-photon interactions in cavity-QED systems have been demonstrated in Ref. [12], where two light beams interact through a QD (InAs) coupled to a cavity in a photonic crystal. In that experiment, the reporting numbers are $g/\gamma_r \sim 1$ and $g/\omega \sim 10^{-4}$. Again, these number are within reach of plasmonic resonators, see Fig. 7.

Other Photon-photon interaction allows exploring Bose-Hubbard-like models in JC-lattices, i.e. arrays of coupled cavity-TLS systems. The non-equally spaced levels in the JC-model can yield two phases – localization and delocalization – depending on the coupling g and the hopping term between the cavities [74]. These phases survive even with dissipation [75]. Cavity QED is also a building block for quantum information tasks. On the other hand demonstrations of quantum computation [76], state tomography [77] or quantum buses [78] were done in systems exceeding the ratios $g/\max[\gamma_r,\gamma_e,\gamma_d]$ presented here. This motivates to further improve current numbers by *e.g.* improving the reflectivities in order to enable these tasks in plasmonic resonators. Finally, we mention recent advances in doing quantum physics driven by dissipation [79, 80]. There, dissipation is viewed as beneficial for reaching interesting ground states or doing quantum computation. Because of strong dissipation present in quantum plasmonics, further investigation in this direction seems rewarding.

6. Conclusions

We have reported a quantum theory for plasmonic resonators coupled to quantum emitters. Starting from a *first principle* theory, and taking into account the main losses, we were able to end up in a master equation for the effective JC model, Cf. Eq. (16). All the coefficients can be obtained via the classical Green's function together with the emitter characteristics. This permits to profit from the studies on plasmonic waveguides. We have studied different architectures for optimizing the binomia of field enhancement and losses to reach the SC regime. We have numerically demonstrated that SC in plasmonics QED is possible at cryogenic temperatures. Albeit it is demanding at room temperature it is possible if further improvements are reached, *e.g.* mirror reflectivities. Importantly enough our calculations agree with recent experimental results in the WC regime with plasmonic resonators made of nanowires, see our section 5.1. Further, we have shown that other architectures, as hybrid or wedge can overcome the nanowire implementation and reaching higher Purcell factos. In the paper we also compare the capabilities of plasmonic resonators with other technologies. As demonstrated plasmonic QED can be used as an effective Kerr media or for generating plasmon-plasmon interactions, demonstrating its feasibility for controlling the few plasmon dynamics at the nanoscale.

Acknowledgments

This work was supported by Spanish MICINN projects FIS2011-25167, MAT2011-28581-C02-02 and CSD2007-046-Nanolight.es. FJGV acknowledges financial support by the European Research Council, grant 290981 (PLASMONANOQUANTA).

Appendix A. EM quantization in dispersive media: the system-environment approach

In this appendix we give a rough overview for the quantization program in dispersive (and therefore also lossy) media. We follow an *open system* approach wherethe losses are modeled by a reservoir (or "bath") accounting for the irreversible leakage of energy from the system. We find a *Quantum Langevin Equation*, that in the classical limit is the Maxwell equation of the EM fields [29, 30].

It is convenient to work both in reciprocal space,

$$\vec{E}(\vec{r},t)=\frac{1}{(2\pi)^{3/2}}\int \mathrm{d}^3k\,\vec{E}(\vec{k},t)\mathrm{e}^{i\vec{k}\cdot\vec{r}}, \tag{A.1}$$

and in the Coulomb Gauge,

$$\nabla\vec{A} = 0\,. \tag{A.2}$$

The quantization is based on a system-bath Lagrangian, where a continuum of bosons $(\vec{x}_j, \vec{p}_j)$ provides an irreversible loss channel,

$$L_{\text{total}} = \varepsilon_0 \int \mathrm{d}^3k \, \left(|\dot{\vec{A}}|^2 - c\vec{k}^2|\vec{A}|^2\right) + \sum_j \left(\mu \dot{x}_j^2 - \omega_j^2 x_j^2\right) + \sum_j \alpha_j \int \mathrm{d}^3k \, \left(\dot{\vec{x}}_j \vec{A}^* + \dot{\vec{x}}_j^{\,*} \vec{A}\right) , \tag{A.3}$$

where we omit the explicit dependence on $\vec{k}$ and t in $\vec{A}(\vec{k},t)$. The introduced constants will later on be identified with the system's material parameters.

With Lagrangian (A.3) at hand we start the quantization of $\vec{A}(\vec{k},t)$ and their conjugate momenta

$$\Pi = \frac{\partial \mathscr{L}}{\partial \dot{\vec{A}}^*} \,, \quad \Pi^* = \frac{\partial \mathscr{L}}{\partial \dot{\vec{A}}} \tag{A.4}$$

The quantized fields satisfy the commutation relations [81]

$$[\vec{A}(\vec{k}), \vec{\Pi}(\vec{k}')] = 0\,, \quad [\vec{A}(\vec{k}), \vec{\Pi}^\dagger(\vec{k}')] = i\hbar\delta(\vec{k} - \vec{k}') \tag{A.5}$$

and the bath's coordinates satisfy

$$[\vec{x}_j, \vec{p}_{j'}] = i\hbar\vec{\delta}_{jj'} \tag{A.6}$$

We write the Heisenberg equations of motion for both $\mathbf{A}$ and the bath operators x_j. Because of the interaction part, [Cf. third term in (A.3)] these equations are coupled

$$\varepsilon_0 \ddot{\vec{A}} = -c^2\vec{k}^2\vec{A} - \sum_j \alpha_j \vec{x}_j \tag{A.7}$$

$$\ddot{\vec{x}}_j = -\omega_j^2 \vec{x}_j + \frac{\alpha_j}{\mu}\dot{\vec{A}}\,. \tag{A.8}$$

The solution of (A.8) is given by

$$\dot{\vec{x}}_j = i\sqrt{\frac{\hbar\omega_j}{2\mu}}\left(f_j^\dagger \mathrm{e}^{i\omega_j t} - f_j \mathrm{e}^{-i\omega_j t}\right) - \frac{\alpha_j}{\mu\omega_j}\int_{-\infty}^{t} \sin(\omega_j(t-t'))\ddot{\vec{A}} \tag{A.9}$$

with the anhilation/creation operatos: $\vec{x}_j = i\sqrt{\hbar\omega_j/2\mu}(f_j^\dagger + f_j)$. Inserting the above (A.9) in (A.7) together with some algebra we end up with an equation for the Fourier components of the vector potential,

$$\vec{A}(\vec{k},t) = \int \mathrm{d}\omega \mathrm{e}^{-i\omega t}\vec{A}_\omega(\vec{k}) \tag{A.10}$$

that can be cast to a *Langevin*-like form

$$-\varepsilon(\omega)\omega^2\vec{A}_\omega = -c^2\vec{k}^2\vec{A}_\omega - i\frac{\hbar}{\pi}\int \mathrm{d}\nu\, \nu\sqrt{\varepsilon''(\nu)}\left(a_\nu^\dagger \mathrm{e}^{i\nu t} - a_\nu \mathrm{e}^{-i\nu t}\right). \tag{A.11}$$

The introduced permittivity of the media

$$\varepsilon(\omega) = \varepsilon'(\omega) + i\varepsilon''(\omega) = 1 + \frac{1}{\varepsilon_0}\left(\mathscr{P}\left[\int \mathrm{d}\nu \frac{J(\nu)}{\nu - \omega}\right] + i\frac{\pi}{2}J(\omega)\right) \tag{A.12}$$

Notice that we have introduced the imaginary part $\varepsilon''(\omega)$ also appearing in the integrand of (A.11) and the spectral density

$$J(\omega) = \sum_j \frac{\alpha_j^2}{\mu\omega_j}\delta(\omega - \omega_j) \tag{A.13}$$

Equations (A.12) and (A.13) link the macroscopic complex permittivity function with a microscopic model accounting for linear dissipation. As a consequence, the fields can be obtained via the Green's function as expressed in Eq. (1) in the main text.

Appendix B. Green's function of resonators

Appendix B.1. Linear resonator

To get the Green's function of a resonator, we first assume that the system is translational along the z-direction with additional reflections at the resonator ends, effectively reducing the problem to one dimension. We further notice that $G_{1\mathrm{d}}(\omega,z,z')$ can be obtained by summing all the waves scattered at the mirrors. A resonator of length L with complex reflection coefficient R ($0 \leq |R| \leq 1$) on the resonator ends located at x_l and x_r therefore yields the 1D Green's function

$$G_{1\mathrm{d}}\left(\omega,z,z'\right) = \sum_{n=0}^{\infty}\left(e^{ik2L}R^2\right)^n \frac{i}{2k}\left(e^{ik|z-z'|}+ Re^{ik|2z_r-(z+z')|}+Re^{-ik|2z_l-(z+z')|}+R^2e^{ik|2L-(z-z')|}\right). \tag{B.1}$$

Without loss of generality we set $z_r = L/2 = -z_l$.

The coupling of an emitter to the resonator, $|g(\omega)|^2 \propto \mathrm{Im}G_{1\mathrm{d}}(\omega,z,z)$, depends on the position z. To maximize the coupling we will consider the emitter to be positioned at an antinode of the electric field.

Appendix B.2. Circular resonator

In the circular resonator configuration the boundary condition is 2π-periodicity. In a similar way as for the linear case summing all the different waves yields the Green's function

$$G_{1\mathrm{d}}\left(\omega,z,z'\right) = \sum_{n=0}^{\infty}\left(e^{ik2}\right)^n \frac{i}{2k}\left(e^{ik|z-z'|}+e^{ik\left(L-|z-z'|\right)}\right). \tag{B.2}$$

Notice that the resonator emitter coupling does not depend on the emitter position.

Appendix B.3. Approximating resonances

By introducing

$$\theta = \theta' + i\theta'' = k'L + \varphi + i\left(k''L - \ln|R|\right) \tag{B.3}$$

where the phase jump at the mirrors, $\varphi = \arg(R)$, is π for the linear resonator and zero in the circular configuration, we can write the 1D-Green's function evaluated at a field antinode and $z = z'$ for both linear and circular resonator as

$$G_{1\mathrm{d}}(\omega,z,z) = \frac{1}{2k}\frac{i\sinh\theta'' + \sin\theta'}{\cosh\theta'' - \cos\theta'} \tag{B.4}$$

We see that θ'' quantifies the losses, both for propagation via the imaginary part of the propagation constant, k'', and the losses through the mirrors via $|R| < 1$. For radiation losses due to bending in the circular resonator we can phenomenologically add a term k''_{bend} to the imaginary part of the propagation constant, k''.

The condition for resonances is

$$L = \frac{\pi}{k'_r}m = \frac{\lambda}{2}m \tag{B.5}$$

where m is the number of antinodes in the resonator and has to be an even integer for circular resonators and any integer for the linear configuration, In both configurations the coupling

$$|g(\omega)|^2 = \Gamma_{\mathrm{guide}}\frac{1}{\pi}\mathrm{Im}\left\{kG_{1\mathrm{d}}(\omega,z,z)\right\}, \tag{B.6}$$

can be approximated by a Lorentzian near a resonance. We approximate the cosine around the center of the resonance peaks

$$\cos(\theta') \cong 1 - \frac{1}{2}L^2(k'-k_0')^2 = 1 - \frac{L^2}{2v_g^2}(\omega-\omega_0) \tag{B.7}$$

Therefore we can write,

$$|g(\omega)|^2 \cong g^2 \frac{1}{\pi} \frac{\gamma_r/2}{(\omega-\omega_0)^2 + (\gamma_r/2)^2}\,. \tag{B.8}$$

with the width of the Lorentzian (FWHM) γ_r being the resonator decay rate

$$\gamma_r = 2\frac{v_g}{L}\sqrt{2(\cosh\theta''-1)} \approx 2\frac{v_g}{L}\theta'' \tag{B.9}$$

and the coupling defined as

$$g = \sqrt{\Gamma_{\text{open}}\frac{v_g}{L}}\sqrt{\frac{\sinh\theta''}{\sqrt{2(\cosh\theta''-1)}}} \approx \sqrt{\Gamma_{\text{open}}\frac{v_g}{L}}\,. \tag{B.10}$$

The approximated results were obtained by assuming weak losses, $\theta'' \ll 1$, and consequently Taylor expanding $\sinh(\theta'')$ and $\cosh(\theta'')$.

For small enough γ_r the Lorentzian (B.8) can be approximated by the peak (13) which is used in the mapping to the Jaynes-Cummings model.

Appendix C. Purcell factors

Applying the Markov approximation, the emitter coupled to a plasmon resonator undergoes exponential decay into surface plasmons with a rate given by the spectral density at the frequency of the emitter, ω_e [82](Fermi's golden rule)

$$\Gamma_{\text{res}} = 2\pi\,|g(\omega_e)|^2\,. \tag{C.1}$$

We define the Purcell factor as the ratio of this emission into surface plasmons compared to Γ_0, the emission if the emitter would be placed in a homogeneous medium characterized by ε_d,

$$F = \frac{\Gamma_{\text{res}}}{\Gamma_0}\,, \tag{C.2}$$

If emission into other channels is negligible small compared to the emission into surface plasmons, this Purcell factor measures the decrease of the emitter lifetime.

In the case of plasmonic resonators the Purcell factor can be written as the product of two different contributions

$$F = \frac{\Gamma_{\text{res}}}{\Gamma_0} = F_{\text{guide}} \times F_{\text{res}}\,. \tag{C.3}$$

The waveguide Purcell Factor F_{guide} exists even without a cavity. It is a result of the small mode area and higher density of states ($\partial k/\partial\omega = v_g^{-1}$) of guided surface plasmons

$$F_{\text{guide}} = \frac{\Gamma_{\text{guide}}}{\Gamma_0} = \frac{3}{\pi\varepsilon_d n_d}\frac{c}{v_g}\frac{A_{\text{free}}}{A_{\text{eff}}}\,. \tag{C.4}$$

Since it has no resonance origin, it is broadband. The additional Purcell factor when building a resonator out of the waveguide, F_{res}, is for $g \ll \max\{\gamma_r, \gamma_p, \gamma_e\}$

$$F_{\text{res}} = \frac{\Gamma_{\text{res}}}{\Gamma_{\text{guide}}} = \frac{4g^2}{\gamma_r+\gamma_d}/\Gamma_{\text{guide}}\,, \tag{C.5}$$

where γ_d is the linewidth due to emitter dephasing (spectral diffusion). Using $g^2 = \frac{v_g}{L}\Gamma_{\text{guide}}$, $\omega = v_p 2\pi/\lambda$ and the quality factors $Q_d = \omega_e/\gamma_d$(emitter dephasing) and $Q_r = \omega_r/\gamma_r$ (resonator) we can rewrite the resonator Purcell factor in terms of

$$F_{\text{res}} = \frac{4}{m\pi}\frac{v_g}{v_p}\frac{1}{\frac{1}{Q_p}+\frac{1}{Q_r}}\,. \tag{C.6}$$

The fraction of emission guided into surface plasmons is given by

$$\beta = \frac{\Gamma_{\text{res}}}{\Gamma_{\text{res}}+\gamma_e} \tag{C.7}$$

In normal cavity QED the emitter decay rates not into the cavity (γ_e) stay approximately the same with and without the cavity since the cavity only affects the modes in a small spatial angle. In plasmonics the presence of the metal surface drastically alters the emission into free modes and additionally adds decay rates into non-radiative modes that dissipate in the metal. Here the plasmonic cavity is quite useful as it increases the decay into surface plasmons and not the decay into non-radiative modes. This is an advantage of the "resonator Purcell factor" over the "broadband Purcell factor".

Appendix D. Temperature and propagation losses

Since the phonon population is strongly temperature dependent, we can significantly reduce scattering of electrons and increase the plasmon propagation lengths.

To get the permittivity as a function of temperature, we recourse to the Drude-Sommerfeld model for free electrons which is well-applicable and sufficient for near infrared to telecom($\lambda_0 \approx 1550\,\text{nm}$) wavelengths, where interband transitions can be safely neglected in silver. Here, the permittivity is given by the plasma frequency of the free electrons ω_p and the damping rate of the electrons Γ_{el}

$$\varepsilon_{\text{Drude}}(\omega) = 1 - \frac{\omega_p^2}{\omega^2 + i\Gamma_{\text{el}}\omega}\,. \tag{D.1}$$

The damping is a function of Fermi velocity v_F and the mean free path of the electrons l_{el}, $\Gamma_{\text{el}} = \frac{v_F}{l_{\text{el}}}$. The mean free path is in turn proportional to the resistivity ρ, $l_{\text{el}} \propto 1/\rho$. Using $\omega \gg \Gamma_{\text{el}}$ the imaginary part of the permittivity is thus approximately proportional to the resistivity

$$\varepsilon''_{\text{Drude}}(\omega) \propto \Gamma_{\text{el}} \propto \rho\,. \tag{D.2}$$

By using tabulated data for the resistivity of silver [83] at different temperatures and scaling Γ_{el} accordingly, we get the imaginary part of the permittivity at different temperatures. The real part stays approximately constant.

With $|\varepsilon'| \gg |\varepsilon''|$ the modal shape of the propagating plasmons is not affected and the reduced imaginary part of the permittivity directly translates into increased propagation length. The imaginary part of the permittivity is plotted in Fig. D1. It translates to a propagation length increase that is universal for all waveguides analyzed in this paper.

At low temperatures ε'' saturates since the dominant electron scattering happens at lattice impurities. Furthermore, when the scattering due to the Drude-Sommerfield model vanishes, the small but maybe finite interband transitions may play a role. Note that at optical frequencies they may even dominate. That is why the change of ε'' is less pronounced for $\lambda_0 = 650\,\text{nm}$ in Fig. D1. However, the data used for interband transitions may be very vague

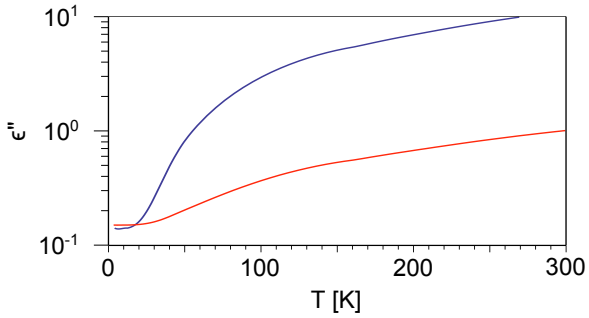

Figure D1. Permittivity of silver as a function of temperature for $\lambda_0 = 1550\,\text{nm}$ (blue line) and $\lambda_0 = 650\,\text{nm}$ (red line). We see that an increase of about 100 is possible in the first case, while an increase of about 10 is possible for optical frequencies.

at lower temperatures since it is obtained from a fit at room temperature. A more close experimental analysis is needed here.

Of special interest are the properties at 77 K and 4 K reachable with liquid nitrogen and liquid helium, respectively. At 77 K an increase of about 5 and at 4 K an increase of about 80 compared to the room temperature propagation lengths can be expected at 1550nm. For purer silver even more may be possible.

References

[1] S. Haroche and J.M. Raimond. Cavity quantum electrodynamics. *Scientific American*, 54:26, 1993.

[2] J. Raimond, M. Brune, and S. Haroche. Manipulating quantum entanglement with atoms and photons in a cavity. *Reviews of Modern Physics*, 73(3):565–582, August 2001.

[3] Xiaobo Zhu, Shiro Saito, Alexander Kemp, Kosuke Kakuyanagi, Shin-ichi Karimoto, Hayato Nakano, William J Munro, Yasuhiro Tokura, Mark S Everitt, Kae Nemoto, Makoto Kasu, Norikazu Mizuochi, and Kouichi Semba. Coherent coupling of a superconducting flux qubit to an electron spin ensemble in diamond. *Nature*, 478(7368):221–4, October 2011.

[4] M D LaHaye, J Suh, P M Echternach, K C Schwab, and M L Roukes. Nanomechanical measurements of a superconducting qubit. *Nature*, 459(7249):960–4, June 2009.

[5] G A Steele, A K Hüttel, B Witkamp, M Poot, H B Meerwaldt, L P Kouwenhoven, and H S J van der Zant. Strong coupling between single-electron tunneling and nanomechanical motion. *Science (New York, N.Y.)*, 325(5944):1103–7, August 2009.

[6] K. Hennessy, A. Badolato, M. Winger, D. Gerace, M. Atatüre, S. Gulde, S. Fält, A. I. EL Hu, et al. Quantum nature of a strongly coupled single quantum dot–cavity system. *Nature*, 445(7130):896–899, 2007.

[7] 478, 2011.

[8] Oriol Romero-Isart, Mathieu L Juan, Romain Quidant, and J Ignacio Cirac. Toward quantum superposition of living organisms. *New Journal of Physics*, 12(3):033015, March 2010.

[9] Nathalie P. de Leon, Brendan J. Shields, Chun L. Yu, Dirk E. Englund, Alexey V. Akimov, Mikhail D. Lukin, and Hongkun Park. Tailoring Light-Matter interaction with a nanoscale plasmon resonator. *Physical Review Letters*, 108(22):226803, May 2012.

[10] Yi Mu and C. M. Savage. One-atom lasers. *Physical Review A*, 46(9):5944–5954, November 1992.

[11] Yi Yin, H. Wang, M. Mariantoni, Radoslaw Bialczak, R. Barends, Y. Chen, M. Lenander, Erik Lucero, M. Neeley, A. O'Connell, D. Sank, M. Weides, J. Wenner, T. Yamamoto, J. Zhao, A. Cleland, and John Martinis. Dynamic quantum Kerr effect in circuit quantum electrodynamics. *Physical Review A*, 85(2), February 2012.

[12] Dirk Englund, Arka Majumdar, Michal Bajcsy, Andrei Faraon, Pierre Petroff, and Jelena Vučković. Ultrafast Photon-Photon Interaction in a Strongly Coupled Quantum Dot-Cavity System. *Physical Review Letters*, 108(9), March 2012.

[13] T D Ladd, F Jelezko, R Laflamme, Y Nakamura, C Monroe, and J L O'Brien. Quantum computers. *Nature*, 464(7285):45–53, March 2010.

[14] T. Niemczyk, F. Deppe, H. Huebl, E. P. Menzel, F. Hocke, M. J. Schwarz, J. J. Garcia-Ripoll, D. Zueco,

T. Hümmer, E. Solano, A. Marx, and R. Gross. Circuit quantum electrodynamics in the ultrastrong-coupling regime. *Nature Physics*, 6(10):772–776, July 2010.

[15] P. Forn-Díaz, J. Lisenfeld, D. Marcos, J. García-Ripoll, E. Solano, C. Harmans, and J. Mooij. Observation of the Bloch-Siegert Shift in a Qubit-Oscillator System in the Ultrastrong Coupling Regime. *Physical Review Letters*, 105(23), November 2010.

[16] D. E. Chang, A. S. Sørensen, P. R. Hemmer, and M. D. Lukin. Strong coupling of single emitters to surface plasmons. *Physical Review B*, 76(3):035420, July 2007.

[17] R F Oulton, G Bartal, D F P Pile, and X Zhang. Confinement and propagation characteristics of subwavelength plasmonic modes. *New Journal of Physics*, 10(10):105018, October 2008.

[18] R. F. Oulton, V. J. Sorger, D. A. Genov, D. F. P. Pile, and X. Zhang. A hybrid plasmonic waveguide for subwavelength confinement and long-range propagation. *Nature Photonics*, 2(8):496–500, July 2008.

[19] Alexandra Boltasseva, Valentyn S. Volkov, Rasmus B. Nielsen, Esteban Moreno, Sergio G. Rodrigo, and Sergey I. Bozhevolnyi. Triangular metal wedges for subwavelengthplasmon-polariton guiding at telecomwavelengths. *Optics Express*, 16(8):5252–5260, April 2008.

[20] Sergey I. Bozhevolnyi, Valentyn S. Volkov, Elo|[iuml]|se Devaux, Jean-Yves Laluet, and Thomas W. Ebbesen. Channel plasmon subwavelength waveguide components including interferometers and ring resonators. *Nature*, 440(7083):508–511, March 2006.

[21] Mark I. Stockman. Nanofocusing of optical energy in tapered plasmonic waveguides. *Phys. Rev. Lett.*, 93:137404, Sep 2004.

[22] V. S. Volkov, S. I. Bozhevolnyi, Sergio G. Rodrigo, L. Martin-Moreno, F. J. Garcia-Vidal, E. Devaux, and Thomas W. Ebbesen. Nanofocusing with channel plasmon polaritons. *Nano Letters*, 9(3):1278–1282, 2009.

[23] Rupert F. Oulton, Volker J. Sorger, Thomas Zentgraf, Ren-Min Ma, Christopher Gladden, Lun Dai, Guy Bartal, and Xiang Zhang. Plasmon lasers at deep subwavelength scale. *Nature*, 461(7264):629–632, August 2009.

[24] D. Martin-Cano, L. Martin-Moreno, F. J. Garcia-Vidal, and E. Moreno. Resonance energy transfer and superradiance mediated by plasmonic nanowaveguides. *Nano Letters*, 10(8):3129–3134, 2010.

[25] A. Gonzalez-Tudela, D. Martin-Cano, E. Moreno, L. Martin-Moreno, C. Tejedor, and F. J. Garcia-Vidal. Entanglement of two qubits mediated by one-dimensional plasmonic waveguides. *Phys. Rev. Lett.*, 106:020501, Jan 2011.

[26] Yiyang Gong and Jelena Vuc?kovic? Design of plasmon cavities for solid-state cavity quantum electrodynamics applications. *Applied Physics Letters*, 90(3):033113, 2007.

[27] Lukas Novotny and Bert Hecht. *Principles of Nano-Optics*. Cambridge University Press, June 2006.

[28] Ulrich Weiss. *Quantum dissipative systems*. World Scientific, June 2008.

[29] Bruno Huttner and Stephen M. Barnett. Quantization of the electromagnetic field in dielectrics. *Physical Review A*, 46(7):4306–4322, October 1992.

[30] T. G. Philbin. Canonical quantization of macroscopic electromagnetism. *New Journal of Physics*, 12:123008, 2010.

[31] Ludwig Knoll, Stefan Scheel, and Dirk-Gunnar Welsch. QED in dispersing and absorbing media. *quant-ph/0006121*, June 2000.

[32] Ho Trung Dung, Ludwig Knöll, and Dirk-Gunnar Welsch. Three-dimensional quantization of the electromagnetic field in dispersive and absorbing inhomogeneous dielectrics. *Physical Review A*, 57(5):3931, May 1998.

[33] Ho Trung Dung, Stefan Yoshi Buhmann, Ludwig Knöll, Dirk-Gunnar Welsch, Stefan Scheel, and Jürgen Kästel. Electromagnetic-field quantization and spontaneous decay in left-handed media. *Physical Review A*, 68(4):043816, October 2003.

[34] T. Gruner and D. G Welsch. Green-function approach to the radiation-field quantization for homogeneous and inhomogeneous Kramers-Kronig dielectrics. *Physical Review A*, 53(3):1818, 1996.

[35] Wolfgang P. Schleich. *Quantum Optics in Phase Space*. Wiley-VCH, 1 edition, February 2001.

[36] Chance R. R., Prock A., , and Silbey R. Molecular fluorescence and energy transfer near interfaces. *Adv. chem. Phys.*, 37:1, 1978.

[37] W. L. Barnes. Fluorescence near interfaces: the role of photonic mode density. *Journal of Modern Optics*, 45:661, 1998.

[38] Yuntian Chen, Torben Roland Nielsen, Niels Gregersen, Peter Lodahl, and Jesper Mørk. Finite-element modeling of spontaneous emission of a quantum emitter at nanoscale proximity to plasmonic waveguides. *Physical Review B*, 81(12):125431, March 2010.

[39] T. Søndergaard and B. Tromborg. General theory for spontaneous emission in active dielectric microstructures: Example of a fiber amplifier. *Physical Review A*, 64(3):033812, 2001.

[40] Chen-To Tai. *Dyadic Green Functions in Electromagnetic Theory*. Oxford University Press, USA, September 1996.

[41] George W. Hanson and Alexander B. Yakovlev. *Operator Theory for Electromagnetics: An Introduction*. Springer, 2002.

[42] A. J. Leggett. Quantum tunneling in the presence of an arbitrary linear dissipation mechanism. *Physical Review*

B, 30(3):1208–1218, 1984.

[43] Anupam Garg, Jose? Nelson Onuchic, and Vinay Ambegaokar. Effect of friction on electron transfer in biomolecules. *The Journal of Chemical Physics*, 83:4491, 1985.

[44] M. C. Goorden, M. Thorwart, and M. Grifoni. Entanglement spectroscopy of a driven Solid-State qubit and its detector. *Physical Review Letters*, 93(26):267005, December 2004.

[45] Liang Xian-Ting. Decoherence and relaxation of a qubit coupled to an ohmic bath directly and via an intermediate harmonic oscillator. *Chemical Physics Letters*, 449(4-6):296–303, December 2007.

[46] Heinz-Peter Breuer and Francesco Petruccione. *The theory of open quantum systems*. Oxford University Press, 2002.

[47] Claude Cohen-Tannoudji, Jacques Dupont-Roc, and Gilbert Grynberg. *Atom-Photon Interactions: Basic Processes and Applications*. Wiley-Interscience, 1992.

[48] A. Auffèves, J. M Gérard, and J. P Poizat. Pure emitter dephasing: A resource for advanced solid-state single-photon sources. *Physical Review A*, 79(5):053838, 2009.

[49] A. Gonzalez-Tudela, E. del Valle, E. Cancellieri, C. Tejedor, D. Sanvitto, and F. P Laussy. Effect of pure dephasing on the Jaynes-Cummings nonlinearities. *arXiv:0907.1302*, July 2009. Optics Express, Vol. 18, Issue 7, pp. 7002-7009 (2010).

[50] A. Auffèves, D. Gerace, J.-M. Gérard, M. França Santos, L. C. Andreani, and J.-P. Poizat. Controlling the dynamics of a coupled atom-cavity system by pure dephasing. *Physical Review B*, 81(24):245419, June 2010.

[51] Guoqiang Cui and M. G. Raymer. Emission spectra and quantum efficiency of single-photon sources in the cavity-QED strong-coupling regime. *Physical Review A*, 73(5):053807, May 2006.

[52] Arka Majumdar, Andrei Faraon, Erik D. Kim, Dirk Englund, Hyochul Kim, Pierre Petroff, and Jelena Vučković. Linewidth broadening of a quantum dot coupled to an off-resonant cavity. *Physical Review B*, 82(4):045306, July 2010.

[53] Esteban Moreno, Sergio G. Rodrigo, Sergey I. Bozhevolnyi, L. Martin-Moreno, and F. J. Garcia-Vidal. Guiding and focusing of electromagnetic fields with wedge plasmon polaritons. *Phys. Rev. Lett.*, 100:023901, Jan 2008.

[54] Wenhui Wang, Qing Yang, Fengru Fan, Hongxing Xu, and Zhong Lin Wang. Light propagation in curved silver nanowire plasmonic waveguides. *Nano Lett.*, 11(4):1603–1608, 2011.

[55] Dirk Jan Dikken, Marko Spasenovi?, Ewold Verhagen, Dries van Oosten, and L. (Kobus) Kuipers. Characterization of bending losses for curved plasmonic nanowire waveguides. *Optics Express*, 18(15):16112–16119, July 2010.

[56] R. F. Oulton, D. F. P. Pile, Y. Liu, and X. Zhang. Scattering of surface plasmon polaritons at abrupt surface interfaces: Implications for nanoscale cavities. *Physical Review B*, 76(3):035408, July 2007.

[57] Kerry J. Vahala. Optical microcavities. *Nature*, 424(6950):839–846, 2003.

[58] G. Rempe, R. J. Thompson, H. J. Kimble, and R. Lalezari. Measurement of ultralow losses in an optical interferometer. *Optics letters*, 17(5):363–365, 1992.

[59] A. Laucht, N. Hauke, J. M. Villas-Bôas, F. Hofbauer, G. Böhm, M. Kaniber, and J. J. Finley. Dephasing of exciton polaritons in photoexcited InGaAs quantum dots in GaAs nanocavities. *Physical Review Letters*, 103(8):087405, 2009.

[60] I. Aharonovich, S. Castelletto, D. A. Simpson, C. H. Su, A. D. Greentree, and S. Prawer. Diamond-based single-photon emitters. *Reports on Progress in Physics*, 74:076501, 2011.

[61] U. Banin, M. Bruchez, A. P. Alivisatos, T. Ha, S. Weiss, and D. S. Chemla. Evidence for a thermal contribution to emission intermittency in single CdSe/CdS core/shell nanocrystals. *The Journal of Chemical Physics*, 110(2):1195–1201, January 1999.

[62] A. V. Akimov, A. Mukherjee, C. L. Yu, D. E. Chang, A. S. Zibrov, P. R. Hemmer, H. Park, and M. D. Lukin. Generation of single optical plasmons in metallic nanowires coupled to quantum dots. *Nature*, 450(7168):402–406, November 2007.

[63] Mads Lykke Andersen, Soren Stobbe, Anders Sondberg Sorensen, and Peter Lodahl. Strongly modified plasmon-matter interaction with mesoscopic quantum emitters. *Nat Phys*, 7(3):215–218, March 2011.

[64] Lucio Claudio Andreani, Giovanna Panzarini, and Jean-Michel Gérard. Strong-coupling regime for quantum boxes in pillar microcavities: Theory. *Physical Review B*, 60(19):13276, November 1999.

[65] Fabrice Laussy, Elena del Valle, and Carlos Tejedor. Strong Coupling of Quantum Dots in Microcavities. *Physical Review Letters*, 101(8), August 2008.

[66] Elena del Valle, Fabrice P. Laussy, and Carlos Tejedor. Luminescence spectra of quantum dots in microcavities. II. fermions. *Physical Review B*, 79(23):235326, June 2009.

[67] H. Ditlbacher, A. Hohenau, D. Wagner, U. Kreibig, M. Rogers, F. Hofer, F.R. Aussenegg, and J.R. Krenn. Silver nanowires as surface plasmon resonators. *Physical review letters*, 95(25):257403, 2005.

[68] Barnes W. L., Dereux A., and Ebbesen T.W. Surface plasmon subwavelength optics. *Nature*, 424:824, 2003.

[69] Ernst Jan R. Vesseur, F. Javier García de Abajo, and Albert Polman. Broadband purcell enhancement in plasmonic ring cavities. *Physical Review B*, 82(16):165419, October 2010.

[70] Mark P. Hiscocks, Chun-Hsu Su, Brant C. Gibson, Andrew D. Greentree, Lloyd C. L. Hollenberg, and François Ladouceur. Slot-waveguide cavities for optical quantum information applications. *Optics Express*, 17(9):7295, April 2009.

[71] David Zueco, Georg Reuther, Sigmund Kohler, and Peter Hänggi. Qubit-oscillator dynamics in the dispersive regime: Analytical theory beyond the rotating-wave approximation. *Physical Review A*, 80(3), September 2009.

[72] Kurt Jacobs and Andrew Landahl. Engineering Giant Nonlinearities in Quantum Nanosystems. *Physical Review Letters*, 103(6), August 2009.

[73] A. Hoffman, S. Srinivasan, S. Schmidt, L. Spietz, J. Aumentado, H. Türeci, and A. Houck. Dispersive Photon Blockade in a Superconducting Circuit. *Physical Review Letters*, 107(5), July 2011.

[74] Dimitris Angelakis, Marcelo Santos, and Sougato Bose. Photon-blockade-induced Mott transitions and XY spin models in coupled cavity arrays. *Physical Review A*, 76(3), September 2007.

[75] Thomas Hümmer, Georg Reuther, Peter Hänggi, and David Zueco. Nonequilibrium phases in hybrid arrays with flux qubits and nitrogen-vacancy centers. *Physical Review A*, 85(5), May 2012.

[76] Matteo Mariantoni, H Wang, T Yamamoto, M Neeley, Radoslaw C Bialczak, Y Chen, M Lenander, Erik Lucero, A D O'Connell, D Sank, M Weides, J Wenner, Y Yin, J Zhao, A N Korotkov, A N Cleland, and John M Martinis. Implementing the quantum von Neumann architecture with superconducting circuits. *Science (New York, N.Y.)*, 334(6052):61–5, October 2011.

[77] Max Hofheinz, H Wang, M Ansmann, Radoslaw C Bialczak, Erik Lucero, M Neeley, A D O'Connell, D Sank, J Wenner, John M Martinis, and A N Cleland. Synthesizing arbitrary quantum states in a superconducting resonator. *Nature*, 459(7246):546–9, May 2009.

[78] J Majer, J M Chow, J M Gambetta, Jens Koch, B R Johnson, J A Schreier, L Frunzio, D I Schuster, A A Houck, A Wallraff, A Blais, M H Devoret, S M Girvin, and R J Schoelkopf. Coupling superconducting qubits via a cavity bus. *Nature*, 449(7161):443–7, September 2007.

[79] S. Diehl, A. Micheli, A. Kantian, B. Kraus, H. P. Büchler, and P. Zoller. Quantum states and phases in driven open quantum systems with cold atoms. *Nature Physics*, 4(11):878–883, September 2008.

[80] Frank Verstraete, Michael M. Wolf, and J. Ignacio Cirac. Quantum computation and quantum-state engineering driven by dissipation. *Nature Physics*, 5(9):633–636, July 2009.

[81] Claude Cohen-Tannoudji, Jacques Dupont-Roc, and Gilbert Grynberg. *Atom-Photon Interactions: Basic Processes and Applications*. Wiley-VCH, March 1998.

[82] Fam Le Kien and K. Hakuta. Cavity-enhanced channeling of emission from an atom into a nanofiber. *Physical Review A*, 80(5):053826, November 2009.

[83] D.R. Smith and FR Fickett. Low-temperature properties of silver. *JOURNAL OF RESEARCH-NATIONAL INSTITUTE OF STANDARDS AND TECHNOLOGY*, 100:119–119, 1995.